BIOMIMETICS

Robotic vertical jumping agility via series-elastic power modulation

Duncan W. Haldane,[1]* M. M. Plecnik,[2] J. K. Yim,[2] R. S. Fearing[2]

Several arboreal mammals have the ability to rapidly and repeatedly jump vertical distances of 2 m, starting from rest. We characterize this performance by a metric we call vertical jumping agility. Through basic kinetic relations, we show that this agility metric is fundamentally constrained by available actuator power. Although rapid high jumping is an important performance characteristic, the ability to control forces during stance also appears critical for sophisticated behaviors. The animal with the highest vertical jumping agility, the galago (*Galago senegalensis*), is known to use a power-modulating strategy to obtain higher peak power than that of muscle alone. Few previous robots have used series-elastic power modulation (achieved by combining series-elastic actuation with variable mechanical advantage), and because of motor power limits, the best current robot has a vertical jumping agility of only 55% of a galago. Through use of a specialized leg mechanism designed to enhance power modulation, we constructed a jumping robot that achieved 78% of the vertical jumping agility of a galago. Agile robots can explore venues of locomotion that were not previously attainable. We demonstrate this with a wall jump, where the robot leaps from the floor to a wall and then springs off the wall to reach a net height that is greater than that accessible by a single jump. Our results show that series-elastic power modulation is an actuation strategy that enables a clade of vertically agile robots.

INTRODUCTION

Humans participating in the sport of parkour opportunistically reach for disparate handholds and footholds on urban features such as walls, banisters, and railings. Arboreal animals leap between branches, and mountain goats bound across cliff faces. The farther a system can leap, the greater is its reach, and the larger the set of available footholds becomes. These are examples of agile behaviors, and at present, robots fall short of the jumping performance shown by these extreme animal locomotors.

Power modulation is an adaptation found in natural systems (and designed into some robotic systems) that increases the peak power available for jumping. Known as power amplification in the biomechanics literature [a misnomer (*1*)], power modulation occurs whenever the instantaneous power developed by a muscle-tendon complex exceeds the maximum available from the muscle alone (*1*). It has been observed across diverse phylogenetic lines in chameleons (*2*), salamanders (*3*), pipefish (*4*), and mantis shrimp (*5*), and its role has been studied to explain the performance of jumping animals (*6*–*9*). During a power-modulating behavior, muscles transfer energy into series-elastic or parallel-elastic structures and then release that stored energy at power levels greater than what the muscle alone can produce. The arrangement of elastic structures determines how power flows from the actuators and how stored potential energy is converted into kinetic energy. To establish how these actuator topologies facilitate agile locomotion, we anchor the study with an agility metric.

Our goal for this metric is that it is defined for both animal and robotic systems and is simple to calculate from purely extrinsic measures (i.e., requires no invasive measurements of muscle force or power). We define vertical jumping agility to be the height that a system can reach with a single jump in Earth gravity, multiplied by the frequency at which that jump can be made. Vertical jumping agility is then equal to $h/(t_{stance} + t_{apogee})$, where h is the jump height, t_{stance} is the total stance time from the onset of actuation, and t_{apogee} is the flight time from when the jumper leaves the ground until the apogee of a jump (when the vertical velocity is zero). This metric can be ascertained from a video of a maximal jump, satisfying the goal of definition by extrinsic measure. This metric is an extension of previous work defining vertical agility as the product of the gravitational constant and the maximum jumping height (*10*). By considering the rate at which platforms can jump, we can more clearly differentiate between systems. Because jumps terminate with zero vertical velocity, a ballistic limit [$h \leq g/(2\omega^2)$, where h is the jump height, ω is the jump frequency, and g is the gravitational constant] is determined when the stance time drops to zero and the platform spends all its time in flight. Other forms of vertical locomotion such as climbing, running uphill, or flapping flight can be described with a vertical agility metric but are not subject to the ballistic limit because the vertical velocity does not reach zero before another cycle occurs.

Vertical jumping agility is measured in vertical meters per second, corresponding to the average vertical speed that a system can attain with repeated jumps (or how quickly a predator would have to chase an animal leaping from branch to branch up a tree). Because it is defined as a climb rate in a gravitational environment, the vertical jumping agility of any system is limited to its power-to-weight ratio. This metric is a dimensional quantity because the jump heights and distances imposed by the environment do not vary with platform size. If locomotion over adverse terrain requires a vertical jump of 1 m, then a 1-m jump is required, regardless of system mass. Vertical jumping agility describes how much and how quickly an animal can change its energetic state; it does not consider planar changes of direction or turning behaviors, which have been addressed by previous work (*11*).

The interplay of jump frequency and height gain is shown in Fig. 1 for three robots using different actuation strategies, as well as the most vertically agile animal for which data were found (*Galago senegalensis*, the lesser galago). This figure shows a series of repeated vertical jumps for each system over an interval of 4.0 s, the time required for one full wind-and-jump cycle by the EPFL (École Polytechnique Fédérale de Lausanne) Jumper (*12*). Over this time interval, the EPFL Jumper

[1]Department of Mechanical Engineering, University of California at Berkeley, CA 94720, USA. [2]Department of Electrical Engineering and Computer Science, University of California at Berkeley, CA 94720, USA.
*Corresponding author. Email: dhaldane@berkeley.edu

jumps once to attain a height of 1.3 m; the more agile galago jumps five times to a height of 8.5 m.

In nature, vertical jumping agility is important for predator-prey interactions, which drive the evolution of specialized performance in both participants (*13*). The choice of prey escape tactic frequently depends on the environment: Anoles encountered at ground level escape by running, whereas those in shrubs prefer to jump (*14*); saxicolous species of snow skinks use jumping; the arboreal species almost invariably climb (*15*); and black-tailed deer stot more frequently when surprised in high vegetation (*16*). The jumping ability of prey animals determines hunting tactics in jumping spiders (*17*), and the vertical jumps of caracals allow them to prey upon birds in flight (*18*). The vertical jumping agility of a prey animal may mediate its success when vertically escaping pursuit; any prey animal escaping upward with multiple jumps (or by climbing) will escape its predator if it has a greater vertical jumping agility. Vertical jumping agility could be a contributor to evolutionary fitness, resulting in model animal systems that can guide the creation of more vertically agile robots. Furthermore, the creation of vertically agile robots may provide biologically relevant insights into animal locomotion.

Figure 2 shows the height gain and jump frequency (defined for a single jump), for a range of animal and robotic systems, as well as hyperbolae of constant vertical jumping agility and the aforementioned ballistic limit of jumping locomotion. All the constant agility curves intersect the ballistic limit, indicating that the highest agilities can only be realized by increasing jump height. The highest observed vertical jumping agility was 2.2 m/s from the galago. The robot developed in this work has an agility of 1.75 m/s, which is higher than that of the previously most agile robot, 1.12 m/s [Minitaur (*19*)]. We will refer to this chart while assessing how the choice of actuation topology has affected vertical jumping agility in robotic systems.

A robotic jumper can use a rigid actuation strategy, with no substantial compliance between the actuators and the environment. Minitaur (*19*) and the MIT (Massachusetts Institute of Technology) Cheetah (*20*) have leveraged the fact that electromagnetic actuators scale favorably with size (*21*) and use rigid, torque-dense actuators. These systems have similar vertical jumping agility and can jump at rates greater than 2 Hz; the more agile of the two (Minitaur) has 54% greater power density than estimates made for the galago (*8*), but half the vertical jumping agility.

All of the animal systems in Fig. 2 have nonnegligible compliance in the muscle-tendon complexes that power their jumps. This compliance enables power modulation and allows them to attain greater vertical jumping agility than robotic jumpers of greater power density. Several robots have incorporated compliant elements [for a survey, see (*22*)]; the robots with nonrigid actuators in Fig. 2 use either parallel-elastic or series-elastic elements.

A parallel-elastic robot has a compliant element attached in parallel with the leg structure, coupling leg extension to energetic state. The disadvantages of this approach are that the position of the leg cannot be changed without doing energetic work and that collision losses are increased (*23*) (should the actuator not be decoupled). As opposed to series-elastic robots, parallel-elastic robots can work to increase their energetic state while airborne, and energy storage is only limited by maximum actuator force and strain energy storage density. Small jumping robots (*12*, *24*–*29*) [inspired by insects using a similar strategy, i.e., (*30*)] use a high-force, low-speed actuator to wind a parallel-elastic leg mechanism (sometimes over a number of minutes) and then decouple the motor, allowing the stored energy to be returned rapidly. This design choice resulted in the highest robotic jumps, but none of the parallel-elastic robots attained a vertical jumping agility greater than 0.34 m/s,

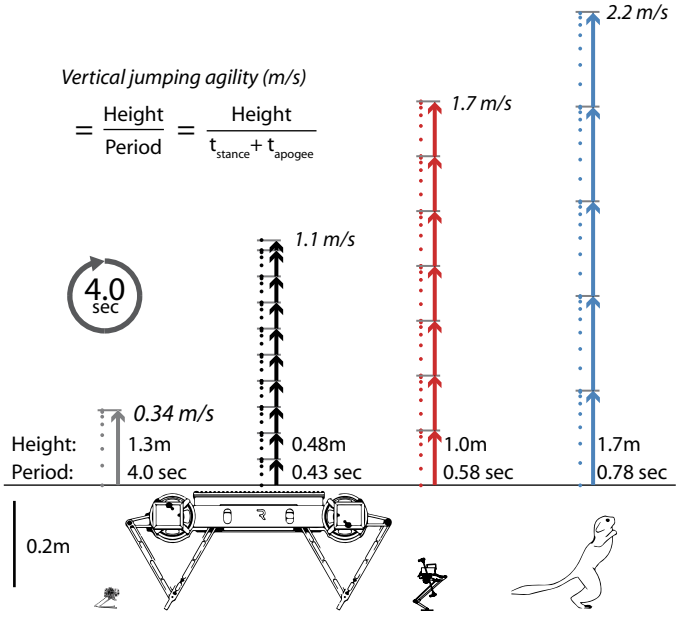

Fig. 1. Four seconds of agile jumping. (**Left** to **right**) A series of jumps for the most agile systems for various actuation strategies: parallel-elastic (EPFL Jumper), rigid (Minitaur), series-elastic power-modulating (this work), and animal (*G. senegalensis*). Each arrow represents one jump; the jump period and height gain are shown next to each series.

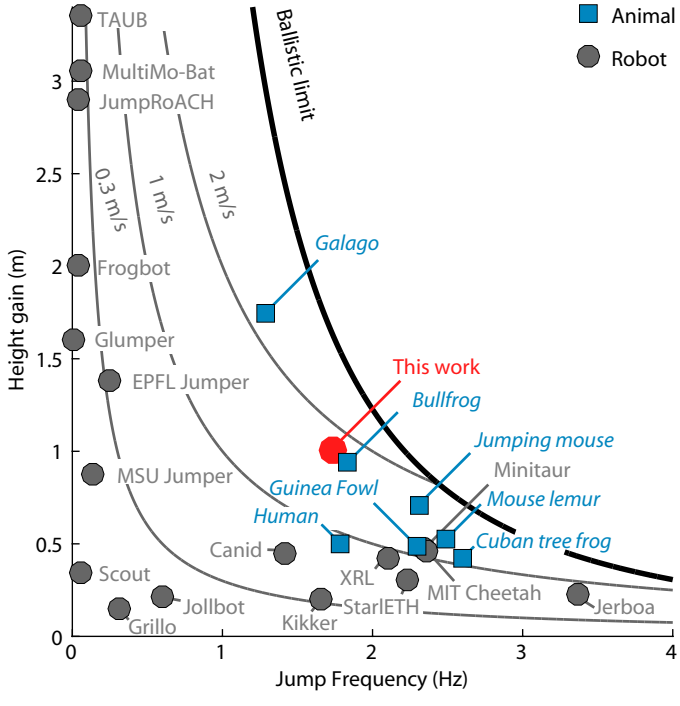

Fig. 2. Height gain and jump frequency for animal and untethered robotic systems. The ballistic limit for jumping and hyperbolae defining constant agility for 0.3, 1, and 2 m/s are also shown. Animal species: *G. senegalensis* [galago (*8*)], *Rana catesbeiana* [bullfrog (*9*)], *Zapus trinotatus* [jumping mouse (*52*)], *Microcebus murinus* [mouse lemur (*53*)], *Osteopilus septentrionalis* [Cuban tree frog (*7*)], *Numida meleagris* [guinea fowl (*6*)], and *Homo sapiens* [human (*54*)]. Data from explosion-powered robots (*55*) are not shown.

with most populating the region near the vertical axis in Fig. 2. The choice of decoupling the actuator to enable rapid energy release means that these parallel-elastic jumpers cannot control power release within a given jump. Previous work with the bow-leg hopper (*31*) has shown that this can be sufficient to control a monoped that has low step-to-step energetic variation.

A series-elastic robot interposes a spring element between a rigid actuator and the environment. This reduces the impedance of the jumping appendage, safeguards a potentially fragile actuator, allows force controllability and passive energy recovery, and enables power modulation (*32*, *33*) without coupling leg position to energetic state. Robots using series-elastic actuators (*34*–*37*) have a greater vertical jumping agility than all of the parallel-elastic systems but less than the rigidly actuated Minitaur and MIT Cheetah. An adaptation has been found in animals adapted for saltatorial locomotion that increases the peak power output of a series-elastic actuator, which could increase robotic vertical jumping agility.

Previous work has shown that a mechanical advantage (MA) adaptation can increase the energy that a series-elastic muscle-tendon complex can deliver (*38*). MA is defined here as the ratio between the reaction force at the foot to the force applied by the actuator. A low MA means that the muscle can apply a high force (which stores energy in the elastic tendon), with low ground contact force, preventing the large upward acceleration that would otherwise result. Animals with pronounced degrees of power modulation have an MA profile that starts low to store energy and then increases throughout the stroke, rapidly releasing energy for high-power jumps (*38*). The magnitude of this effect is shown by the galago, whose jump requires 15 times more power than its muscles alone produce (*8*). A robotic series-elastic actuator with an MA adaptation (SE+MA) would use a series-elastic actuator to drive a limb with an MA profile designed to increase the energy delivered over the stroke, more than what would be otherwise realizable. This strategy preserves the benefits of a series-elastic actuator, which are well matched to the task of agile locomotion. Previous work (*39*) with a tethered SE+MA prototype has proved the concept of this approach, showing that the appendage could deliver 3.6 times more power than the motor alone could produce.

Any robot that drives a leg with nontrivial kinematics using a series-elastic actuator [such as the proposed Skippy (*40*)] is capable of power-modulating behavior. However, to the authors' knowledge, a treatment involving designing the MA profile of a limb to increase the energy that it can deliver and experimental evidence of the efficacy of this approach have yet to be presented. We seek an understanding of how the fundamental choice of actuation strategy affects vertical jumping agility and engineering methods by which an SE+MA actuator can be instantiated in a physical prototype. We also seek to explore vertical jumping agility–enabled behaviors using a robotic prototype with an SE+MA appendage, Salto.

RESULTS

We first explored the interplay between actuation strategy and vertical jumping agility using a model of an SE+MA system that is shown in Fig. 3A. Here, a mass (M) was driven by a series-elastic actuator composed of a linear motor (force: $F = F_{max} - VF_{max}/V_{max}$, where V is actuator velocity) and a linear spring of stiffness k that applied force to the ground through a transmission with an MA [$G(x_l)$] that is a function of leg extension. We created a robotic platform (Salto) to experimentally evaluate power modulation. Figure 3B shows a diagram of a linkage synthesized to instantiate an SE+MA MA profile. Salto, shown in Fig. 3C, was used to perform experiments including vertical jumps and a wall jump maneuver.

Designing a robotic galago

All current robots fall short of the galago's vertical jumping agility. The following design study explains this shortfall by evaluating the power density (peak mechanical power per unit mass) that robotic systems would require to match the galago's performance. The mass and leg extension have been fixed to that of the galago (0.25 kg and 0.15 m, respectively), and we explored the choice of rigid, parallel-elastic, series-elastic, and SE+MA actuators for two different power densities. The rigid and parallel-elastic actuators have been idealized as constant power motors, thus including robotic designs with specialized transmissions [like Grillo (*28*)]. Our prototype will not have a specialized transmission; to closer match reality, the series-elastic and SE+MA designs use the previously presented linear motor model. The SE+MA MA function that we explored was piecewise constant, starting leg extension with a low MA to store energy and ending with a high MA to return it. This adaptation is parameterized by G_R, the ratio of ending MA to starting MA.

Figure 4 shows rigid, parallel-elastic, series-elastic, and SE+MA jumpers for power densities of 10 and 100 W/kg, in the vertical jumping agility metric space. Along each curve are points that correspond to various values of G_R; the series-elastic design without an MA adaptation occurs at $G_R = 1$. The design points in Fig. 4 were determined by optimizing for vertical jumping agility over all free parameters.

A galago has a power density of about 93 W/kg (*8*). Figure 4 shows that the highest jump for a galago (100 W/kg) with ideal rigid actuators would only be 0.68 m, a 60% reduction in height, with a vertical jumping agility of only 1.8 m/s.

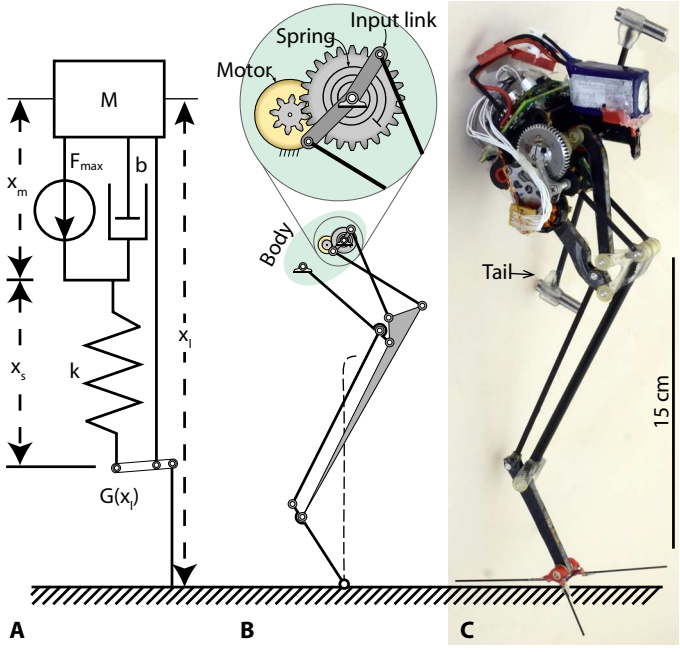

Fig. 3. Power modulation modeled and instantiated. (**A**) Model of a power-modulating system with a series-elastic actuator and an MA element. (**B**) Linkage schematic for the robotic mechanism. (**C**) Photograph of an integrated robotic platform, Salto.

Both series-elastic and SE+MA systems can jump higher than a rigid jumper of the same power density. The actuator delivers energy to the elastic element instead of directly accelerating the body; this extends stance time and thus the net energy delivered (*32*, *33*). The energy in the elastic element can be returned without power limit, and SE+MA designs converged to a limit wherein the starting MA was low enough that gravity prevented extension of the leg until a large amount of energy was stored and the ending MA rapidly returned the energy. Increasing the MA ratio increased the jump height for SE+MA systems. The vertical jumping agility for the 10-W/kg case does not increase substantially with this gain in jump height, which is fundamentally limited to a vertical jumping agility of 1.0 m/s {10 W/[(1 kg) 9.81 m s^{-2}]}, the equivalent constant-speed elevator limit. The 100-W/kg system sees substantial gains in agility as the MA ratio is increased; the SE+MA actuator allows more energy to be delivered. The agility curve associated with this power density lies outside the bounds of Fig. 4.

The hypothetical parallel-elastic jumper continuously applies constant power, winding in the air and in stance [similar to Grillo (*28*) and the bow-leg hopper (*41*)], and returns that power as an impulse. This jumper would operate along the ballistic limit until the intersection with the vertical agility curve defined by that jumper's power-to-weight ratio and then trace that constant vertical agility curve. Physically, this corresponds to jumping with zero stance times until hitting the power-to-weight limit and then increasing jump height by increasing stance time. The 10-W/kg parallel-elastic robot in Fig. 4 would operate along the curve of agility = 1 m/s, with the intersection point with the ballistic limit beyond the extent of the graph. The 10-W/kg power-modulating jumper asymptotically approaches this limit. The galago's vertical jumping agility could be attained by the constant-power wind-up jumper with a power density of only 21.9 W/kg. However, this achievement implies that force can only be applied as an impulse, whereas the other actuation strategies retain the capacity to control force.

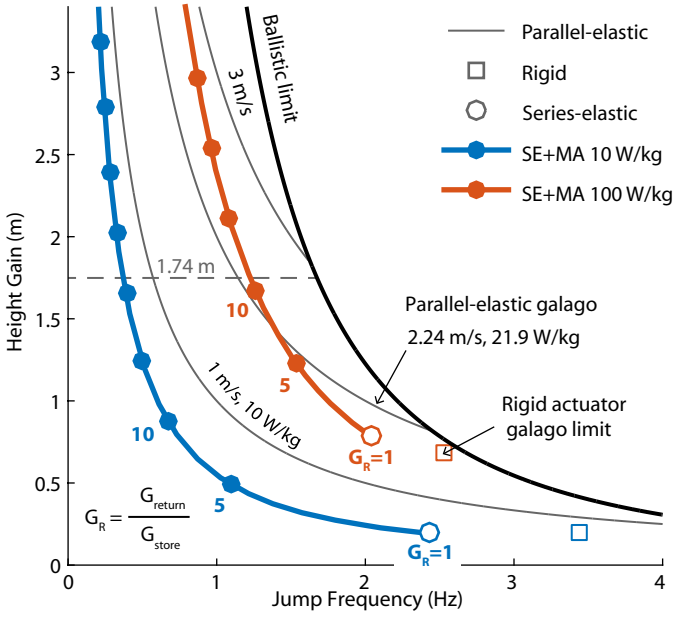

Fig. 4. The effect of actuation on vertical jumping agility. Design points for rigid, parallel-elastic, series-elastic, and SE+MA jumpers for a galago-scale robot (mass, 0.25 kg; leg extension, 0.15 m) are shown. Dots correspond to locations of MA ratio G_R = 1, 5, 10, 15, etc.

We can design a hypothetical robotic galago for each actuation strategy. For this robot, the jump height, mass, and leg extension match data inferred for a galago (*8*). If there are sufficient parameters, the vertical jumping agility matches that of the galago; otherwise, the vertical jumping agility is left unconstrained. Given these constraints, we then determine the minimum power density requisite for the jump, specifying that the system starts with zero energy.

The result of the design study is shown in Table 1, with data from the galago and experimental results from Salto. The rigid and basic series-elastic systems needed the highest power densities to match the jump height of the galago. The higher power densities of these systems resulted in lower stance times for the jumps (as compared with SE+MA), resulting in higher vertical jumping agility. The series-elastic system required a lower power density than the rigidly actuated system, because the spring enabled power modulation, as has been previously observed (*32*, *42*); the parallel-elastic robot needed a much lower power. No parallel-elastic robot has attained this performance; thus, we present data from the most vertically agile parallel elastic robot (EPFL Jumper) for comparison. The hypothetical SE+MA robot has the lowest required power density of the actuation strategies that do not preclude force controllability, falling close to an estimate of galago power density by Aerts (*8*). The rigid and series-elastic cases are strict subsets of the SE+MA system; hence, it is expected that the SE+MA system would do at least as well. However, the degree of improvement is substantial; it requires 3.8 times less power density than the rigid actuator and 3.6 times less power density than the optimized series-elastic actuator without an MA adaptation. The series arrangement of the actuator allows it to apply power through the stance phase.

A robotic prototype applying power modulation

We built a physical robotic prototype, Salto (shown in Fig. 3C), to experimentally examine power modulation and its effect on locomotory performance. The result of the design methodology is a monopedal jumper composed of a linkage that enables power modulation, a series-elastic actuator, and an inertial tail for attitude control. Salto was designed to minimize mass so that less energy is required per unit height gain and to improve robustness against high-energy collisions created by agile locomotion. Physical parameters of Salto are given in Table 1. It jumps in free space, with neither tether nor planarizing boom, both of which might interfere with agile motions.

We use a planar eight-bar revolute linkage (shown in Fig. 3B) to encode an MA profile enabling power modulation, as well as fundamental attributes that decouple leaping motions from rotational dynamics. We conceptualize the MA (shown in Fig. 5) as piecewise constant for the purpose of designing an SE+MA jumping appendage. The profile starts low at 2.49 N/Nm in the energy storage phase and increases to an average of 26.90 N/Nm in the energy return phase, with a G_R value of 10.8. To limit damaging peak forces during energy release, we specify that the MA function produces a constant force when the leg mechanism leaves the energy storage phase, reducing the peak acceleration (~20*g*) by a factor of 2, as compared with a constant-MA case.

We also specify that extension of the leg generates no body rotation to enforce decoupled dynamics. This was accomplished by specifying that the foot moves along a straight line that passes through the center of gravity of the linkage and the robot body, as shown by the dashed line in Fig. 3B. This consideration was included in the linkage synthesis process, as described in Materials and Methods.

A series-elastic actuator composed of a torsional spring and geared brushless DC motor drives the linkage. For energy density

Table 1. Actuation strategies for designing a hypothetical robotic galago.

	Galago (*8*)	Hypothetical rigid	Hypothetical series-elastic	Hypothetical parallel-elastic	Hypothetical SE +MA	EPFL Jumper	Salto
Mass (kg)	0.250	0.250	0.250	0.250	0.250	0.007	0.1000
Leg length (m)	0.15	0.15	0.15	0.15	0.15	0.1	0.15
Maximum jump height (m)	1.74	1.74	1.74	1.74	1.74	1.38	1.008
Jump frequency (Hz)	1.29	1.66	1.59	1.29	1.29	0.248	1.74
Vertical jumping agility (m/s)	2.24	2.89	2.78	2.24	2.24	0.34	1.75
Power density (W/kg)	92.7 (estimated)	343	325	21.9	90	50	137

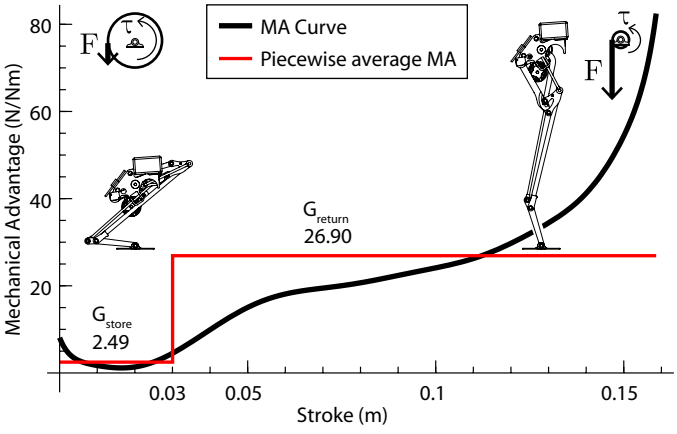

Fig. 5. MA as a function of leg extension. Average values of G_{store} and G_{return} for energy storage and return phases are shown. Cartoons show the leg mechanism fully crouched and fully extended.

and compactness, the conic-sectioned torsional latex spring developed for the SEA snake (Series Elastic Actuator snake) (*43*) was used. This design fully loads the elastic material and leverages the latex's higher energy storage per unit mass compared with other common spring materials such as composites or steel.

The final component of the robot is an inertial tail for pitch reorientation. This strategy is used by leaping agama lizards (*44*) and has been used in several other robotic platforms (*25*, *45*, *46*). In contrast to these other systems, which use an unbalanced distal mass, our tail is mass-balanced about its point of rotation [similar to the KAIST (Korea Advanced Institute of Science and Technology) Raptor]. This decouples the angular position of the tail from the center of mass location of the system. Furthermore, it allows the use of a smaller tail motor that would be otherwise overwhelmed by torques generated by characteristically large accelerations developed in stance phase. More details on the robotic platform are presented in Materials and Methods.

Robotic experiments

To measure the vertical jumping agility of the platform and determine the efficacy of the SE+MA strategy, we performed a series of vertical jumping experiments to determine the maximum height gain that the robot could achieve. The robot was equipped with a lightweight foot (visible in Fig. 3C) to statically stabilize out-of-plane rotation. The maximum jump height was 1.008 ± 0.007 m (N = 10, mean ± 1 SD). The average stance time was 0.1223 ± 0.0006 s, and the average flight time to apogee was 0.4533± 0.0015 s, for a frequency of 1.74 Hz and an average vertical jumping agility of 1.75 m/s. This point is shown in Fig. 2, demonstrating that Salto has achieved the highest vertical jumping agility of any extant robot.

To anchor the meaning of vertical jumping agility in the context of locomotion, we demonstrate a wall jump with the Salto robotic prototype. In this experiment, the robot starts in a stable configuration on the floor, uses the tail to orient itself toward the wall, jumps, reorients, and then jumps again off the wall. Parameters for this jump were tuned to maximize the height gained off the wall. The motor and spring power are shown in Fig. 6A for the starting jump and in Fig. 6B for the wall contact phase.

Figure 6A shows motor and spring power as a function of time for the robot jumping from its fully crouched position. This figure shows the effect of the SE+MA appendage on power modulation. Eight consecutive trials are shown on this plot, with the time axis starting with the onset of motor activation. The leg stays in the low-MA region (shown in Fig. 5) until 0.06 s into the stroke, loading energy into the spring. After this point, the MA increases and the energy in the spring is returned to accelerate the robot. The average (N = 8) peak spring and motor power were 40.3 ± 1.54 and 13.7 ± 0.0 W, respectively, showing that the spring provided 2.94 times greater power than the motor alone can produce. These data also show the consistency of the power-modulating behavior when the platform starts from rest.

When jumping off the wall, the power-modulating effect is less prominent because contact is made with the leg extended out of the energy storage region, as shown in Fig. 6B. Integrating the motor power shows that an average of 1.22 ± 0.01 J was delivered during the starting jump, and 1.04 ± 0.03 J was delivered during the wall contact phase. Variation in initial conditions when the robot contacts the wall caused this phase to be more variable than the starting jump.

The wall jump was based on internal measurements, with a state machine governing the transitions between the phases of the maneuver. Without a controller operating on exteroceptive measures, this is an open-loop behavior; thus, variability is expected to grow over time. Figure 7A shows motion-tracked position traces for the eight consecutive wall jump maneuvers, with the robot shown for scale. The starting jump produced closely grouped trajectories for the robot approaching the wall, the variation resulting from differences in tail action during

stance. The trajectories diverge after the robot contacts the wall, as can be seen in Fig. 7 (A to C). This greater variability is driven by discrepancies in foothold location and body orientation relative to the wall. Figure 7D is a bar chart showing the extrinsic energetic state of the robot before and after the wall contact phase. Each wall jump increased the energetic state of the robot from an average of 0.96 ± 0.03 to 1.21 ± 0.06 J. The average energy gain from the wall contact phase was 0.25 ± 0.04 J; thus, the variation in extrinsic energy increases with each phase of the wall jump, but the variability of energy production for both phases was similar. We can estimate the efficiency of the starting jump and wall contact phase as the ratio of energy delivered by the motor to the increase in kinetic and potential energy. The starting jump had an average efficiency of 79 ± 3%, on par with other jumping robots (*47*); the wall contact phase had a lower efficiency of 24 ± 4%, presumably dissipating energy through collision with the wall.

The robot attained an average height gain of 1.21 ± 0.065 m for the wall jump, reaching an average of 0.4 m higher than the foothold location on the wall. The maximum height increase was 1.29 m, 0.28 m higher than the maximum achievable were the platform jumping from the floor.

DISCUSSION

A bioinspired series-elastic power-modulating strategy was tested with a robotic prototype, resulting in the highest recorded robotic vertical jumping agility: 1.75 m/s. Salto's vertical jumping agility was higher than that of a bullfrog but fell short of the vertical jumping agility of the galago (2.24 m/s).

Power modulation enables agile robots by reducing the motor power density required to perform energetic jumps. An optimal design study showed that any system with rigid or series-elastic actuators lacking an MA adaptation requires excessive power densities (more suited to hovering flight than legged locomotion), if they are to perform as well as the galago. A hypothetical piecewise constant MA adaptation, coupled with a series-elastic actuator, created a power-modulating system that reduced the required power density by a factor of 3.6, making a robot with the agility of a galago physically realizable.

An alternative to an SE+MA actuator is the sort of parallel-elastic device that propels the highest-jumping robots in Fig. 2. The required power density (assuming spring winding during both stance and flight phases) is less than that required for an SE+MA actuator. However, there are several shortcomings associated with the parallel-elastic approach. These are perhaps best analyzed in the context of the wall jump maneuver. The wall jump requires two repeated, controlled jumps. Parallel-elastic mechanisms typically require position control to set spring length and force and can thus complicate leg force production. An SE+MA actuator preserves force control authority by maintaining the actuator in a series arrangement. During the wall jump, Salto retracted the leg near the free-running speed of the motor to prepare for wall contact. This would not have been possible with a comparable parallel-elastic mechanism because of the energetic work required to change leg position. The robot's ability to perform a high-power jump, rapidly reposition its leg, and jump again off a wall was enabled by the choice of an SE+MA actuation strategy.

The SE+MA leg had repeatable performance, as shown by the power curves in Fig. 6 and the small height variation in the vertical jump experiments. It also had predictable behavior—identical inputs producing similar outputs. The deviations in trajectories shown in Fig. 7 are not due to some inherent flaw in the mechanism but rather result from the lack of a true closed-loop controller for the behavior.

The robot was able to gain height by jumping off the wall, using an environmental feature to increase its operational space. This maneuver can be seen as the first stage of a vertical chute ascent, which was first demonstrated by ParkourBot in its limited gravity environment (*48*).

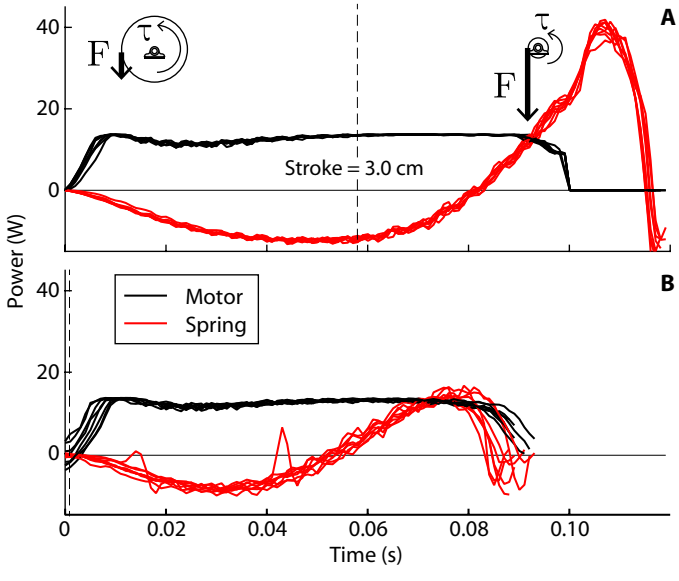

Fig. 6. Spring and motor power during jumps. Spring and motor power for (**A**) the starting jump of the wall jump maneuver and (**B**) the wall contact phase ($N = 8$). The dashed line indicates where the leg moves from the storage to return MA regions (shown in Fig. 5).

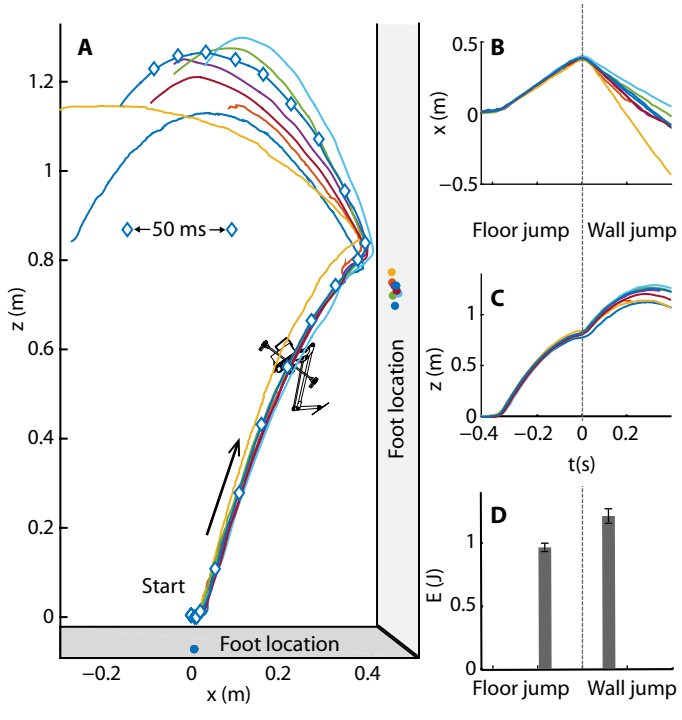

Fig. 7. Trajectories of the robotic wall jump experiments. (**A**) Trajectory of the body center of mass for eight consecutive wall jumps. (**B**) Horizontal displacement versus time. (**C**) Vertical displacement versus time. (**D**) Bar chart of the energy of the robot before and after the wall contact phase. Error bars indicate 1 SD.

This wall jump is an example of a maneuver enabled by highly vertically agile robots.

The main limitation of the experimental study is that the robot can only perform planar maneuvers. All of the actuation for leg extension and inertial reorientation is concentrated in the sagittal plane, and any perturbation away from this plane cannot be rejected. The robot was only operated on hard surfaces with reliable traction; how it would interact with real-world environments and granular media would be an interesting topic of study. The robot only had access to proprioceptive measures, with no capacity to reason about features in the environment and its pose relative to them. The wall jump behavior was open-loop in that sense, being regulated by a set of parameters tuned to produce a reliable behavior.

The study of series-elastic power modulation showed that it is an actuation strategy well suited to agile robots and a viable alternative to parallel-elastic actuation. These results are broadly applicable to robotic locomotion. More directly, the leg mechanism developed in this work can be coupled with a hip mechanism to form the legs of an agile polypedal robot. The vertical jumping agility metric forms a basis of comparison for agile motions, allowing further exploration of robotic actuation strategies. Our goal is that series-elastic power modulation will enable further study of highly agile robotic locomotion.

MATERIALS AND METHODS

Objectives

The objective of this study was to evaluate SE+MA as a principle for increasing robotic vertical jumping agility. Here, we describe how optimal design points were found, how we synthesized a mechanism with a specified MA profile, and the fabrication and experimental methodologies.

Optimal design of jumping systems

The series-elastic and SE+MA designs in Fig. 4 were determined by specifying mass, leg extension, power density, and the MA ratio and optimizing for agility over F_{max}, G_{store}, spring stiffness k, and transition point. The rigid case was solved analytically.

The minimum power density values in Table 1 were determined using a grid search subject to the maximum leg extension constraint and minimum takeoff velocity for the galago's jump height. The rigid jumper was parameterized by its power; all other jumpers were parameterized by linear motor parameters F_{max} and V_{max}. The series-elastic jumper had a spring stiffness, and the SE+MA jumper had both spring stiffness and MA profile. Each parameter set was simulated in Earth gravity starting from rest and zero displacement. The parallel-elastic system was solved analytically.

Synthesis of leg mechanism

The SE+MA leg mechanism was synthesized using an approach described by Plecnik *et al.* (*49*); we give a summary here. The purpose of the leg mechanism is to transform spring torque into a specified ground reaction force that acts through the center of mass of the prototype. The space of engineering solutions that we explored was mechanical linkages composed of revolute joints. The challenge of this design paradigm is that the parameters are embedded in a highly nonlinear geometric space. We approach this challenge with a two-stage method starting with an initial design exploration, followed by a kinematic tuning (*49*, *50*).

Design exploration determines locations in the design space where required behaviors are coarsely achieved. This was accomplished by formulating polynomial synthesis equations and solving them with the homotopy continuation solver Bertini. Kinematic tuning begins with one of these locations and then optimizes to satisfy all requirements to the granularity desired. To begin design exploration, we identified a set of primary required behaviors: (i) the mechanism constrains the foot point to a straight line, the line of action; (ii) foot stroke is long; (iii) pivots are located above the foot with the input near the line of action; and (iv) link lengths are compact.

Using the design procedure outlined by Plecnik and McCarthy (*50*), an atlas of Stephenson six-bar linkages was generated, marking locations of the design space to explore. The design that best produced the primary behaviors was advanced to the kinematic tuning phase to include an extended list of behaviors: (v) the input link attached to the series-elastic actuator rotates over a large range; (vi) a low starting MA; (vii) MA defines a constant force at the foot during the rest of stroke; and (viii) moments exerted on the body are minimized. The optimization was performed using the InteriorPoint method within Mathematica's FindMinimum function.

We dynamically simulated (using approximations of link mass and inertia) a maximal jump to determine the success of the synthesis approach and the magnitude of internal reaction forces and then designed a spring-driven prototype. Experiments with this prototype validated the design of the energy-storing spring, but inaccurate estimations of link masses caused the jumping motion to generate substantial angular momentum. Accurate mass models from the prototype showed that our six-bar design was difficult to balance in order to satisfy (viii) above. Two more links were added to the six-bar linkage, and optimization was performed again to arrive at the final design shown in Fig. 3B. A spring-driven prototype of this refined linkage verified that the design was balanced.

Fabrication and operation of robotic prototype

Simulations show that the leg linkage produced internal forces up to 210 N. To minimize mass, as much of the linkage as possible was made from carbon fiber composite materials. Links in compression or bending were milled from prefabricated honeycomb core carbon fiber composite plates (XS-LP-39, ACP Composites) using a Dremel 569D bit installed in an enclosed precision desktop mill (OtherMill, Other Machine Co.). The torsional stiffness of these sandwich composite members was increased by adhering a 0.005-inch-thick FR-4 fiberglass sheet cut on a 45° bias (1331T23, McMaster-Carr), across the width of the beams with cyanoacrylate adhesive (Loctite 495). The two links that carry purely tensile loads were fabricated as tie rods with unidirectional pultruded carbon fiber flat stock (2153T21, McMaster-Carr). The revolute joints of the mechanism were formed by a precision ground 2024 aluminum rod (9062K24, McMaster-Carr) riding in polymer bushings (JFM-0304-05, igus Inc.). The bushings and shafts were integrated with the structural carbon fiber using molded polyurethane components (IE-3075, Innovative Polymers). A two-stage casting process produced these parts, wherein a solid wax mold was cut using OtherMill, a silicone mold is taken from this positive, and the final polyurethane parts are cast from the silicone mold. This fabrication paradigm resulted in a linkage weighing only 11 g that can withstand the internally generated forces and that did not fail during experiments. Figure S1 shows a three-dimensional (3D) portable document format (pdf) of the robot (without control electronics).

The torsional spring was cut from continuous-dip processed latex (5234K681, McMaster-Carr) into a conic section using a 3D printed jig. Spring material properties and a model for leg friction were identified

by fixing the motor position and cyclically compressing the leg in an Instron material testing machine.

The brushless motor started as a Scorpion S-1804-1650KV winding kit obtained from the factory, wound with 48 turns of 30 AWG (American wire gauge) magnet wire. We statically verified the torque constant. The custom wound stator was mounted in a custom 25:1 gearbox for a total mass of 25.29 g. An AS5047P magnetic encoder calibrated to rotor position generated commutation signals for a current controlling brushless DC motor driver (AZB10A4, *ADVANCED* Motion Controls). The reference was generated by an Imageproc robot control board (*51*) (printed circuit board: https://github.com/biomimetics/imageproc_pcb, firmware: https://github.com/dhaldane/roach). A second AS5048B magnetic encoder measured the angle of the lower ternary link; the angular deflection of the spring was estimated with an inverse-kinematics look-up table. The system was powered by a three-cell 11.1-V 180 mA·hour lithium polymer battery (Turnigy nano-tech).

The control board recorded telemetry (six-axis inertial measurement unit, estimated body angle, leg position, and motor position) at 1000 Hz. It was controlled from a laptop via an onboard ZigBee radio interface. The robot was controlled with two independent linear feedback laws: a proportional controller on motor position and a proportional-derivative controller on body angle. Body angle was estimated by integrating a single axis on the onboard gyroscope. The controller for the wall jump was implemented as a state machine. When started, it sets the pitch set point forward to angle the robot toward the wall. Once the pitch angle reaches a threshold, leg extension is triggered and the robot jumps. In the air, the robot retracts its leg, and the pitch set point is set to the angle at which the robot should contact the wall. Contact with the wall is detected by either the spring displacement exceeding a threshold or the rotational rate of the robot exceeding a threshold. This detector ensemble is more robust against variations in the angle of incidence with the wall than either detector in isolation. Once wall contact is detected, leg extension is again triggered and the robot jumps off the wall.

Experimental procedure

For the vertical jumping tests, the robot was placed on the floor with the center of mass directly above the foot; a step input was then applied to the motor position that drove the jumping linkage to full extension. The tail was not activated for these trials, precluding a controlled landing. The robot was caught by hand after it reached apex. This procedure was repeated for 10 consecutive trials. Movie S1 is a compilation of the vertical jumping videos. The wall jump was performed consecutively for eight trials until the robot failed to perform the maneuver. This failure resulted from damage accrued by the inertial tail, causing the robot to fail to properly orient itself toward the wall. The battery was returned to a full state of charge before each wall jump to isolate sources of experimental variability. The robot was placed 0.59 m away from the wall; markers on the ground ensured repeatable alignment. The wall in these experiments consisted of a 0.25-inch-thick acrylic plate mounted to an extruded aluminum frame. To increase traction, a 0.175-m diameter of 0.25-inch-thick polyurethane rubber was added 0.88 m above the floor, where the robot's foot was expected to make contact. The frictional coefficient was such that Salto's foot did not slip during any of the trails. In addition to telemetry, video footage of each experiment was recorded at 500 fps using a Mega Speed HHC X7. Video tracking software (ProAnalyst, Xcitex) was used to extract kinematics from each experiment. Movie S2 is a compilation of the wall jumping videos.

Motor power was calculated using the current command sent by the Imageproc using the identified motor model and measurements of motor speed. The spring power was estimated by approximating the torque from the spring deflection using estimated spring stiffness and multiplying that estimate by the measured rate of change of spring angle. The extrinsic energy of the system during the wall jump was estimated from the kinematic tracking data.

SUPPLEMENTARY MATERIALS

robotics.sciencemag.org/cgi/content/full/1/1/eaag2048/DC1
Fig. S1. Three-dimensional pdf of robotic prototype Salto.
Movie S1. Vertical jump experiments.
Movie S2. Wall jump experiments.
Data S1. Zip archive of experimental telemetry and processing scripts.
Data S2. Zip archive of experimental videos.

REFERENCES AND NOTES

1. T. J. Roberts, E. Azizi, Flexible mechanisms: The diverse roles of biological springs in vertebrate movement. *J. Exp. Biol.* **214**, 353–361 (2011).
2. J. H. de Groot, J. L. van Leeuwen, Evidence for an elastic projection mechanism in the chameleon tongue, *Proc. Biol. Sci.* **271**, 761–770 (2004).
3. S. M. Deban, J. C. O'Reilly, U. Dicke, J. L. van Leeuwen, Extremely high-power tongue projection in plethodontid salamanders. *J. Exp. Biol.* **210**, 655–667 (2007).
4. S. Van Wassenbergh, J. A. Strother, B. E. Flammang, L. A. Ferry-Graham, P. Aerts, Extremely fast prey capture in pipefish is powered by elastic recoil. *J. R. Soc. Interface* **5**, 285–296 (2008).
5. S. N. Patek, B. N. Nowroozi, J. E. Baio, R. L. Caldwell, A. P. Summers, Linkage mechanics and power amplification of the mantis shrimp's strike. *J. Exp. Biol.* **210**, 3677–3688 (2007).
6. H. T. Henry, D. J. Ellerby, R. L. Marsh, Performance of guinea fowl *Numida meleagris* during jumping requires storage and release of elastic energy. *J. Exp. Biol.* **208**, 3293–3302 (2005).
7. R. L. Marsh, H. B. John-Alder, Jumping performance of hylid frogs measured with high-speed cine film. *J. Exp. Biol.* **188**, 131–141 (1994).
8. P. Aerts, Vertical jumping in Galago senegalensis: The quest for an obligate mechanical power amplifier. *Philos. Trans. R. Soc. London Ser. B* **353**, 1607–1620 (1998).
9. H. C. Astley, E. M. Abbott, E. Azizi, R. L. Marsh, T. J. Roberts, Chasing maximal performance: A cautionary tale from the celebrated jumping frogs of Calaveras County. *J. Exp. Biol.* **216**, 3947–3953 (2013).
10. J. M. Duperret, G. D. Kenneally, J. L. Pusey, D. E. Koditschek, Towards a comparative measure of legged agility, in *Springer Tracts in Advanced Robotics* (Springer International Publishing, 2016), pp. 3–16.
11. R. L. Hatton, L. J. Burton, A. E. Hosoi, H. Choset, Geometric maneuverability with applications to low Reynolds number swimming, in *2011 IEEE/RSJ International Conference on Intelligent Robots and Systems* (IEEE, 2011), pp. 3893–3898.
12. M. Kovac, M. Fuchs, A. Guignard, J.-C. Zufferey, D. Floreano, A miniature 7g jumping robot, in *IEEE International Conference on Robotics and Automation* (IEEE, 2008), pp. 373–378.
13. T. Y. Moore, A. A. Biewener, Outrun or outmaneuver: Predator–prey interactions as a model system for integrating biomechanical studies in a broader ecological and evolutionary context. *Integr. Comp. Biol.* **55**, 1188–1197 (2015).
14. M. Lattanzio, Escape tactic plasticity of two sympatric *Norops* (Beta *Anolis*) species in Northeast Costa Rica. *Amphibia-Reptilia* **30**, 1–6 (2009).
15. J. Melville, R. Swain, Evolutionary correlations between escape behaviour and performance ability in eight species of snow skinks (*Niveoscincus*: Lygosominae) from Tasmania. *J. Zool.* **261**, 79–89 (2003).
16. T. Stankowich, R. G. Coss, Effects of risk assessment, predator behavior, and habitat on escape behavior in Columbian black-tailed deer. *Behav. Ecol.* **18**, 358–367 (2007).
17. M. Bartos, Alternative predatory tactics in a juvenile jumping spider. *J. Arachnol.* **36**, 300–305 (2008).
18. R. H. N. Smithers, thesis, University of Pretoria (1971).
19. G. Kenneally, A. De, D. E. Koditschek, Design principles for a family of direct-drive legged robots. *IEEE Robot. Autom. Lett.* **1**, 900–907 (2016).
20. H.-W. Park, S. Park, S. Kim, Variable-speed quadrupedal bounding using impulse planning: Untethered high-speed 3D running of MIT Cheetah 2, in *2015 IEEE International Conference on Robotics and Automation* (IEEE, 2015), pp. 5163–5170.
21. S. Seok, A. Wang, M. Y. Chuah, D. J. Hyun, J. Lee, D. M. Otten, J. H. Lang, S. Kim, Design principles for energy-efficient legged locomotion and implementation on the MIT Cheetah robot. *IEEE/ASME Trans. Mechatronics* **20**, 1–13 (2014).
22. B. Vanderborght, A. Albu-Schaeffer, A. Bicchi, E. Burdet, D. G. Caldwell, R. Carloni, M. Catalano, O. Eiberger, W. Friedl, G. Ganesh, M. Garabini, M. Grebenstein, G. Grioli, S. Haddadin, H. Hoppner, A. Jafari, M. Laffranchi, D. Lefeber, F. Petit, S. Stramigioli, N. Tsagarakis, M. Van Damme, R. Van Ham, L. C. Visser, S. Wolf, Variable impedance actuators: A review. *Rob. Auton. Syst.* **61**, 1601–1614 (2013).

23. Y. Yesilevskiy, C. D. Remy, W. Xi, A comparison of series and parallel elasticity in a monoped hopper. *IEEE Int. Conf. Robot. Autom.* **2015**, 1036–1041 (2015).
24. J. Burdick, P. Fiorini, Minimalist jumping robots for celestial exploration. *Int. J. Rob. Res.* **22**, 653–674 (2003).
25. J. Zhao, T. Zhao, N. Xi, F. Cintron, M. Mutka, L. Xiao, Controlling aerial maneuvering of a miniature jumping robot using its tail, in *2013 IEEE/RSJ International Conference on Intelligent Robots and Systems* (IEEE, 2013), pp. 3802–3807.
26. S. A. Stoeter, P. E. Rybski, M. Gini, N. Papanikolopoulos, Autonomous stair-hopping with scout robots. *IEEE Int. Conf. Intell. Robot. Syst.* **1**, 721–726 (2002).
27. R. Armour, K. Paskins, A. Bowyer, J. Vincent, W. Megill, R. Bomphrey, Jumping robots: A biomimetic solution to locomotion across rough terrain. *Bioinspir. Biomim.* **2**, S65–S82 (2007).
28. F. Li, W. Liu, X. Fu, G. Bonsignori, U. Scarfogliero, C. Stefanini, P. Dario, Jumping like an insect: Design and dynamic optimization of a jumping mini robot based on bio-mimetic inspiration. *Mechatronics* **22**, 167–176 (2012).
29. T. Tsuda, H. Mochiyama, H. Fujimoto, Quick stair-climbing using snap-through buckling of closed elastica. *Int. Symp. Micro-NanoMechatronics Hum. Sci.*, 368–373 (2012).
30. G. P. Sutton, M. Burrows, Biomechanics of jumping in the flea. *J. Exp. Biol.* **214**, 836–847 (2011).
31. G. Zeglin, B. Brown, Control of a bow leg hopping robot. *IEEE Int. Conf. Robot. Autom.* **1**, 793–798 (1998).
32. A. Galantis, R. C. Woledge, The theoretical limits to the power output of a muscle-tendon complex with inertial and gravitational loads. *Proc. R. Soc. London Ser. B* **270**, 1493–1498 (2003).
33. D. Paluska, H. Herr, The effect of series elasticity on actuator power and work output: Implications for robotic and prosthetic joint design. *Rob. Auton. Syst.* **54**, 667–673 (2006).
34. A. M. Johnson, D. E. Koditschek, Toward a vocabulary of legged leaping, in *2013 IEEE International Conference on Robotics and Automation* (IEEE, 2013), pp. 2568–2575.
35. A. Brill, A. De, A. Johnson, D. Koditschek, Tail-assisted rigid and compliant legged leaping, in *2015 IEEE/RSJ International Conference on Intelligent Robots and Systems* (IEEE, 2015), pp. 6304–6311.
36. C. Gehring, S. Coros, M. Hutter, R. Siegwart, An optimization approach to controlling jump maneuvers for a quadrupedal robot, paper presented at Dynamic Walking 2015, Columbus, OH, 20 to 24 July 2015, abstr. 33.
37. G. C. Haynes, J. Pusey, R. Knopf, A. M. Johnson, D. E. Koditschek, Laboratory on legs: An architecture for adjustable morphology with legged robots, in *Proceedings of SPIE* (SPIE, 2012), p. 83870W.
38. T. J. Roberts, R. L. Marsh, Probing the limits to muscle-powered accelerations: Lessons from jumping bullfrogs. *J. Exp. Biol.* **206**, 2567–2580 (2003).
39. D. W. Haldane, M. Plecnik, J. K. Yim, R. S. Fearing, A power modulating leg mechanism for monopedal hopping, in *IEEE/RSJ International Conference on Intelligent Robotics and Systems* (IEEE, 2016), pp. 4757–4764.
40. J. J. M. Driessen, thesis, TU Delft (2015).
41. B. Brown, G. Zeglin, The bow leg hopping robot, in *Proceedings of the 1998 IEEE International Conference on Robotics and Automation* (IEEE, 1998), pp. 781–786.
42. D. Paluska, H. Herr, Series elasticity and actuator power output, in *Proceedings of the 2006 IEEE International Conference on Robotics and Automation* (IEEE, 2006), pp. 1830–1833.
43. D. Rollinson, S. Ford, B. Brown, H. Choset, Design and modeling of a series elastic element for snake robots, in *Proceedings of the ASME 2013 Dynamic Systems and Control Conference* (ASME, 2013), p. v001T08A002.
44. T. Libby, T. Y. Moore, E. Chang-Siu, D. Li, D. J. Cohen, A. Jusufi, R. J. Full, Tail-assisted pitch control in lizards, robots and dinosaurs. *Nature* **481**, 181–184 (2012).
45. N. J. Kohut, D. Zarrouk, K. C. Peterson, R. S. Fearing, Aerodynamic steering of a 10 cm high-speed running robot, in *2013 IEEE/RSJ International Conference on Intelligence Robots and Systems* (IEEE, 2013), pp. 5593–5599.
46. N. J. Kohut, A. O. Pullin, D. W. Haldane, D. Zarrouk, R. S. Fearing, Precise dynamic turning of a 10 cm legged robot on a low friction surface using a tail, in *2013 IEEE International Conference on Robotics and Automation* (IEEE, 2013), pp. 3299–3306.
47. G.-P. Jung, C. S. Casarez, S.-P. Jung, R. S. Fearing, K.-J. Cho, An integrated jumping-crawling robot using height-adjustable jumping module, in *2016 IEEE International Conference on Robotics and Automation* (IEEE, 2016), pp. 4680–4685.
48. A. Degani, A. W. Long, S. Feng, H. B. Brown, R. D. Gregg, H. Choset, M. T. Mason, K. M. Lynch, Design and open-loop control of the ParkourBot, a dynamic climbing robot. *IEEE Trans. Robot.* **30**, 705–718 (2014).
49. M. M. Plecnik, D. W. Haldane, J. K. Yim, R. S. Fearing, Design exploration and kinematic tuning of a power modulating jumping monopod. *J. Mech. Robot.*, 10.1115/1.4035117 (2016).
50. M. M. Plecnik, J. M. McCarthy, Design of Stephenson linkages that guide a point along a specified trajectory. *Mech. Mach. Theory* **96**, 38–51 (2016).
51. S. S. Baek, F. L. Garcia Bermudez, R. S. Fearing, Flight control for target seeking by 13 gram ornithopter, in *2011 IEEE/RSJ International Conference on Intelligent Robots and Systems* (IEEE, 2011), pp. 2674–2681.
52. T. H. Harty, thesis, Oregon State University (2010).
53. P. Legreneur, F.-R. Thévenet, P.-A. Libourel, K. M. Monteil, S. Montuelle, E. Pouydebat, V. Bels, Hindlimb interarticular coordinations in *Microcebus murinus* in maximal leaping. *J. Exp. Biol.* **213**, 1320–1327 (2010).
54. M. F. Bobbert, Dependence of human squat jump performance on the series elastic compliance of the triceps surae: A simulation study. *J. Exp. Biol.* **204**, 533–542 (2001).
55. P. Weiss, Hop…Hop…Hopbots!: Designers of small, mobile robots takes cues from grasshoppers and frogs. *Sci. News* **159**, 88–91 (2001).

Acknowledgments: We thank the University of California at Berkeley mechanical engineering machine shop for their advice on fabricating the gearbox and the reviewers of this article for their insightful feedback. **Funding:** This work was supported by the U.S. Army Research Laboratory under the Micro Autonomous Systems and Technology Collaborative Technology Alliance, by the NSF under grant CMMI-1549667, and by the NSF Graduate Research Fellowship Program. **Competing interests:** All authors of this paper are inventors on a patent application submitted by the University of California that covers the jumping system and associated software described in this paper. **Author contributions:** D.W.H. created the agility metric, collated background research, identified the galago and series-elastic power modulation as inspirations for a robotic platform, designed and fabricated the robotic prototype and experimental setup, assembled the electronics and wrote the firmware, performed the experiments, and wrote the paper. M.M.P. wrote the computational synthesis routines, designed the kinematics of the leg mechanism, and wrote the associated methods. J.K.Y. calculated optimal jump parameters and power densities for jumping actuation strategies, derived agility and power bound expressions for rigid and wind-up jumpers, built dynamic simulations for robot design and wall jump trajectory selection, assisted in physical experiments, and processed experiment telemetry. R.S.F. directed the research and edited the paper. **Data and materials availability:** Source code and hardware are available on GitHub; telemetry and related scripts are in
data S1, and data S2 contains experimental videos.

Submitted 8 July 2016
Accepted 29 September 2016
Published 6 December 2016
10.1126/scirobotics.aag2048

Citation: D. W. Haldane, M. M. Plecnik, J. K. Yim, R. S. Fearing, Robotic vertical jumping agility via series-elastic power modulation. *Sci. Robot.* **1**, eaag2048 (2016).

Science Robotics

Robotic vertical jumping agility via series-elastic power modulation

Duncan W. Haldane, M. M. Plecnik, J. K. Yim, and R. S. Fearing

Sci. Robot. **1** (1), eaag2048. DOI: 10.1126/scirobotics.aag2048

Science Robotics (ISSN 2470-9476) is published by the American Association for the Advancement of Science. 1200 New York Avenue NW, Washington, DC 20005. The title *Science Robotics* is a registered trademark of AAAS.